AGU PUBLICATIONS

JGR

Journal of Geophysical Research: Atmospheres

RESEARCH ARTICLE
10.1002/2014JD022970

Key Points:
- Fossil fuel and biomass combustion emissions' light absorption properties were quantified
- The OC fraction of fossil and biomass emissions can absorb strongly at UV wavelengths
- PAX results correlate with an aethalometer when filter artifact corrections are considered

Supporting Information:
- Text S1, Tables S1–S5 and Figures S1–S11
- Additional supplementary file

Correspondence to:
J. J. Schauer,
jjschauer@wisc.edu

Citation:
Olson, M. R., M. Victoria Garcia, M. A. Robinson, P. Van Rooy, M. A. Dietenberger, M. Bergin, and J. J. Schauer (2015), Investigation of black and brown carbon multiple-wavelength-dependent light absorption from biomass and fossil fuel combustion source emissions, *J. Geophys. Res. Atmos.*, *120*, doi:10.1002/2014JD022970.

Received 9 DEC 2014
Accepted 5 JUN 2015
Accepted article online 9 JUN 2015

Investigation of black and brown carbon multiple-wavelength-dependent light absorption from biomass and fossil fuel combustion source emissions

Michael R. Olson[1], Mercedes Victoria Garcia[1], Michael A. Robinson[2], Paul Van Rooy[1], Mark A. Dietenberger[3], Michael Bergin[4], and James Jay Schauer[1]

[1]Environmental Chemistry and Technology Program, University of Wisconsin-Madison, Madison, Wisconsin, USA, [2]Cummins Emission Solutions, Stoughton, Wisconsin, USA, [3]Forest Products Laboratory, USDA Forest Service, Madison, Wisconsin, USA, [4]School of Civil and Environmental Engineering, Georgia Institute of Technology, Atlanta, Georgia, USA

Abstract Quantification of the black carbon (BC) and brown carbon (BrC) components of source emissions is critical to understanding the impact combustion aerosols have on atmospheric light absorption. Multiple-wavelength absorption was measured from fuels including wood, agricultural biomass, coals, plant matter, and petroleum distillates in controlled combustion settings. Filter-based absorption measurements were corrected and compared to photoacoustic absorption results. BC absorption was segregated from the total light extinction to estimate the BrC absorption from individual sources. Results were compared to elemental carbon (EC)/organic carbon (OC) concentrations to determine composition's impact on light absorption. Multiple-wavelength absorption coefficients, Angstrom exponent (6.9 to <1.0), mass absorption cross section (MAC), and Delta C (97 $\mu g\,m^{-3}$ to ~0 $\mu g\,m^{-3}$) were highly variable. Sources such as incense and peat emissions showed ultraviolet wavelength (370 nm) BrC absorption over 175 and 80 times (respectively) the BC absorption but only 21 and 11 times (respectively) at 520 nm wavelength. The bulk EC $MAC_{EC,\lambda}$ (average at 520 nm = 9.0 ± 3.7 $m^2\,g^{-1}$; with OC fraction <0.85 = ~7.5 $m^2\,g^{-1}$) and the BrC OC mass absorption cross sections ($MAC_{BrC,OC,\lambda}$) were calculated; at 370 nm ultraviolet wavelengths; the $MAC_{BrC,OC,\lambda}$ ranged from 0.8 $m^2\,g^{-1}$ to 2.29 $m^2\,g^{-1}$ (lowest peat, highest kerosene), while at 520 nm wavelength $MAC_{BrC,OC,\lambda}$ ranged from 0.07 m2 g^{-1} to 0.37 $m^2\,g^{-1}$ (lowest peat, highest kerosene/incense mixture). These MAC results show that OC content can be an important contributor to light absorption when present in significant quantities (>0.9 OC/TC), source emissions have variable absorption spectra, and nonbiomass combustion sources can be significant contributors to BrC.

1. Introduction

Understanding the optical properties of carbonaceous source emissions, quantifying their relative contribution, and segregating the black carbon (BC) and brown carbon (BrC) contribution from combustion sources are essential to improving emission inventories and estimating impacts on atmospheric warming, snowpack deposition, and human exposure. The term black carbon has not been used consistently throughout the literature, but in general, it can be described as a solid carbonaceous material formed during combustion, which strongly absorbs light at all visible wavelengths, is highly refractory, and is quantified by optical methodologies (e.g., aethalometer, particle soot absorption photometer (PSAP), and photoacoustic) [*Andreae and Gelencser*, 2006; *Bond et al.*, 2013]. In this manuscript BC is specifically the aerosol component optically quantified by light absorption at 880 nm and its projection to other wavelengths using an Angstrom exponent of 1, whereas elemental carbon (EC) is quantified via a thermochemical method incorporating an optical correction. Brown carbon is the fraction of carbonaceous aerosols, excluding black carbon, which absorbs light primarily at the low visible wavelengths and the near ultraviolet range of the spectrum. BrC is composed of organic carbon (OC) often associated with biomass burning, including tar materials from smoldering fires, and humic-like substances [*Feng et al.*, 2013]. In this manuscript, organic carbon with a fraction that can preferentially absorb in the UV region is considered BrC [*Bergin et al.*, 2015]. Both BC and BrC have been shown to likely have significant radiative forcing impacts on the Earth's atmospheric energy balance; however, there are a number of uncertainties in the optical properties used to estimate the source impacts when applied to emission inventories [*Bond and Bergstrom*, 2006; *Feng et al.*, 2014; *Schulz et al.*,

2006]. In order to address these uncertainties, optical properties of BrC have been derived using Mie theory to fit observation data or derived through the application of absorption Angstrom exponents (AAE), which are representative of source types including pure EC, biomass burning, and mineral dust [*Bahadur et al*., 2012; *Chung et al*., 2012b; *Feng et al*., 2013]. Adding to the uncertainty, bottom-up radiative forcing models often simplify the BC and BrC absorption components from sources due to the limited availability and complexity of applying multiple-wavelength source specific absorption characteristics from carbonaceous aerosols [*Schulz et al*., 2006]. A key provision to further address the uncertainties in these models is improved and detailed multiple-wavelength absorption properties from atmospherically relevant carbonaceous aerosol sources.

Wavelength-dependent absorption is often used as an indicator of source contribution to ambient particulate matter (PM), for example, the contribution from woodsmoke [*Herich et al*., 2011; *Sandradewi et al*., 2008b]. The AAE, the power law coefficient approximating the change in measured absorption at a given visible light wavelength, and Delta C (Delta $C = UVBC_{370\,nm} - BC_{880\,nm}$ reported by the aethalometer) have been shown to increase when PM has a significant contribution from biomass combustion [*Herich et al*., 2011; *Wang et al*., 2012, 2010]. However, the impacts of other sources such as coal, kerosene, and diesel on AAE and Delta C have not been thoroughly investigated [*Sandradewi et al*., 2008b; *Wang et al*., 2010]. Even without a detailed understanding of nonwoodsmoke impacts on the AAE and Delta C values, researchers have started to question the interpretation of woodsmoke concentrations from aethalometer results [*Harrison et al*., 2013].

Multiple-wavelength light extinction measurements can be obtained in semireal time using a seven-channel aethalometer, a filter-based attenuation method [*Arnott et al*., 2005; *Hansen et al*., 1984; *Snyder and Schauer*, 2007]. The filter-based method is widely deployed, offering long-term monitoring data at numerous locations with relatively low operational cost and effort. The aethalometer, however, has been shown to exhibit systematic errors associated with filter loading, scattering, and matrix interferences, which have led to numerous correction techniques that have been demonstrated to reasonably address the drawbacks associated with the filter-based method [*Arnott et al*., 2005; *Bond et al*., 1999a; *Coen et al*., 2010; *Jimenez et al*., 2007; *Weingartner et al*., 2003]. To correct instrument-reported data, these methods often require a filter tape advancement to establish a reference point without particle loading and apply empirically derived correction factors based on optical properties such as aerosol albedo at a single wavelength. These requirements are obtainable for long-term ambient monitoring but may not be feasible for source samples collected under closed-system conditions and steady state flow balance. During source sampling, a tape advancement can introduce unneeded uncertainty due to altered flow conditions or result in lost data points during the tape advancement period. Additionally, empirically derived correction factors may not be appropriate for unique source samples that can demonstrate unique scattering and absorption characteristics across the visible light spectrum as compared to well-mixed and aged ambient aerosols.

Several studies have investigated the light absorption properties of source emissions; however, these studies have often been limited to single wavelengths, reporting only the bulk mass absorption cross section (MAC), and constrained by a limited number of source emissions types [*Bond et al*., 1999b, 2002; *Shen et al*., 2013; *Singh et al*., 2014]. In this study we apply a simple multiple-linear regression correction to address the filter loading artifact and to adjust for multiple-wavelength particle scattering artifact to develop a robust set of absorption coefficients and cross sections from both biogenic and fossil fuel-derived combustion emissions. The multiple-wavelength absorption results are investigated to understand the relative importance these sources can have on BC and BrC emissions and, through the segregation of the EC and OC, the aerosol's composition contribution to light absorption.

2. Material and Methods

2.1. Sample Collection

Three separate source sampling configurations were applied to obtain samples from a heavy-duty diesel engine, solid biomass and fossil fuels, and small-scale biomass and liquid fossil fuel combustion sources. Sample configurations for these combustion sources required specific dilution sampling systems conducive to the source emission type and rate. Numerous other source testing investigations have

employed similar techniques to collect fresh emissions, so each sample configuration will only be briefly discussed. Diesel samples were collected from a constant volume sampler (CVS) emission tunnel (Cummins Emission Solutions, Stoughton, WI) in which a subsample stream of primary diluted exhaust was introduced to a residence time chamber and completely mixed with filtered and dried secondary dilution air [*Liu et al*., 2008; *Robinson et al*., 2014]. The secondary diluted sample was passed through a Dekati thermodenuder (TD, Dekati, Kangasala, Finland) at one of two temperature set points, 30°C as the nondenuded conditions and 300°C as a denuded condition. Flow through the denuder was maintained at 20 L min^{-1} until distributed to the continuous measurement instruments and filter substrates. *Robinson et al*. [2015] provide a detailed description of the dilution sampler configuration applied to diesel engine emissions [*Robinson et al*., 2015]. It should be noted that while the TD was useful in the development of varied aerosol composition, TD versus non-TD samples could not be directly compared due to particle loss. Supplemental materials document particle loss experiment of NaCl atomization under varied TD temperature regimes. In these experiments, particle loss could exceed 25% from non-TD conditions. Similar losses were observed during source testing, where TD tests resulted in significant OC reduction as intended but also high level of EC reduction. For this reason, caution should be taken when interpreting optical properties of source emission aerosols undergoing TD conditioning.

Solid biomass and fossil fuel combustion emission samples were collected in an open-hood sample system (U.S. Department of Agriculture (USDA) Forest Product Laboratory, Madison, WI) with a controlled primary dilution mass flow rate [*Grexa et al*., 2011]. The sample was secondary diluted by introducing a subsample stream of the primary diluted emissions to a completely mixed residence time chamber with desiccated, high-efficiency particulate air (HEPA) filtered, and activated carbon scrubbed, compressed laboratory air. Based on a flow velocity transect across the dilution tunnel, the substream sample inlet opening was placed at a distance of one-third tunnel diameter from the sidewall (13.5 cm) and sized to approximate isokinetic sampling conditions. The secondary diluted sample from the residence time chamber was further diluted with the conditioned laboratory dilution air and passed through a URG 440 Teflon coated aluminum cyclone (URG Corp. Chapel Hill, NC) at 40.7 L min^{-1} to create an approximate size cut of PM < 0.5 μm. The size-segregated sample flow was then split with 10.7 L min^{-1} passing through the TD at either 30°C or 300°C and distributed to the optical instrumentation and filter substrates; the remaining flow passed through sample filter media. The cyclone size cut was chosen to allow a representative sample size distribution across multiple-combustion sources, sources in which the particle number is dominated by PM with aerodynamic diameters less than 500 nm. Additionally, based on a simple Mie theory model for black carbon, the optical properties of PM do not drastically change with particle size beyond this size cut, and thus measured values are both representative and controlled across sources.

Small-scale liquid and biomass source samples were combusted directly in a sealed 450 L glove box with an internal mixing fan. Figure S1 in the supporting information shows a schematic of the glove box setup. Dry HEPA filtered, and activated carbon scrubbed, laboratory air was directly introduced to the glove box as the primary dilution air, while similarly prepared medical air from compressed gas cylinders was used for secondary dilution. Secondary diluted samples were then size segregated via the URG cyclone, passed through the TD, and distributed to optical instrumentation and filter media.

2.2. Sample Configuration

Combustion emissions were sampled and monitored in a similar manner after being passed through the TD. The diluted source emission was distributed through a sampling manifold to each of the optical instruments including a seven-channel AE-31 aethalometer (Magee Scientific, Berkley, CA), a nephelometer (Radiance Research, Seattle, WA), and a photoacoustic extinctiometer (PAX 532 and 870, Droplet Measurement Technologies, Boulder CO). Particle number concentration was monitored with a TSI Scanning Mobility Particle Sizer (TSI 3080 Electrostatic Classifier, TSI 3010 Condensation Particle Counter, and TSI 3081 differential mobility analyzers, TSI Inc. Shoreview, MN) to monitor particle size distribution during emission tests. PM was collected on prebaked 47 mm quartz fiber filters (Pall Life Sciences, Port Washington, NY) placed in aluminum filter holders equipped with a stainless steel support screen and an 8.55 cm^2 stainless steel definer ring.

Sampling for all configurations was performed in the following manner to ensure near-steady state sampling conditions. All emission sources were prestarted and maintained at similar operating conditions as those

used during testing periods allowing systems to come to "hot start" conditions. Solid fuel combustion was maintained under an active flame condition, and fuel was added near continuously replacing consumed fuel during the test. The kerosene lamp and incense were operated as recommended by the manufacture. Flow equilibrium with the dilution air was established in dilution tunnels and residence time chambers. Once a hot, near-steady state condition was established in the sample systems, the AE31 tape would be advanced ensuring a clean filter tape at the start of the sample run. At the completion of the AE31 flow and light source checks, the AE31 was set to begin automatic sampling. Approximately 30 s prior to the AE31 initiating data logging, the vacuum pumps to the filters were turned on, flushing the manifold system of dilution air and introducing sample laden air to the instrumentation. Prior to all test runs, dilution air was monitored with optical equipment to ensure that no particle number, absorption, or scattering was detected by the real-time instrumentation.

2.3. Filter Collection and Analysis

Samples were collected on prebaked quartz fiber filters, with critical orifice controlled collection flow rates directly from the optical property sample manifold. This ensured that the filter-based measurements were representative of optical instrumentation measurements, eliminating the concerns of PM size variability, dilution uncertainties associated with source sampling methodology, and particle loss that can occur in the TD. Quartz filters were analyzed via National Institutes of Safety and Health (NIOSH) 5040 EC/OC method with a Sunset Laboratory Lab OC-EC Aerosol Analyzer (Sunset Laboratory, Tigard OR) at the Wisconsin State Laboratory of Hygiene (Madison, WI). All OC values were average loading blank subtracted; dynamic blanks were collected with dilution air under comparable sample time periods and did not show significant EC/OC concentrations above the loading blanks. EC/OC uncertainties were propagated to mass concentration levels; in particular, EC uncertainty included error associated with the total pyrolyzed carbon as reported by the NIOSH 5040 method [*Dutton et al*., 2009; *Schauer et al*., 2003].

2.4. Optical Instrumentation

The optical instrumentation used during emission monitoring has been discussed in detail by numerous researchers. All of the instruments, with the exception Droplet Measurement Technologies' PAX, are widely used in the monitoring community. The PAX is a relatively new commercially available instrument, but even so the principles in which the PAX operate have been reported upon widely, and thus the instrumentation will only be briefly discussed in the context of this research [*Anderson et al*., 1996; *Arnott et al*., 2005, 1999; *Bond and Bergstrom*, 2006; *Hansen et al*., 1984; *Heintzenberg and Charlson*, 1996; *Lewis et al*., 2008; *Massabo et al*., 2013; *Schmid et al*., 2006; *Utry et al*., 2013; *Yelverton et al*., 2014]. The AE31 measures BC by collecting a PM sample on a quartz fiber filter tape and measures wavelength-specific attenuation of light across a spot of PM deposition. The attenuation over a sample collection period is proportional to the PM loading on the filter, as related by an applied specific attenuation cross section of the aerosol. The filter loading is then used to calculate a sample concentration, reported as mass per volume of BC, based on the spot area and the volume of air passing through the filter. A 5 min sampling time base, a maximum attenuation of 100 before tape advancement, and a nominal flow rate of 1.5 L min^{-1} were employed during source sampling. The nominal flow used by the AE31 was sensitive to source sampling conditions; specifically, a drop in pressure at the sampling manifold resulted in a pressure drop across the sample inlet and ambient air. This condition resulted in two problematic flow conditions: (1) a quantifiable leak occurred postfilter tape, resulting in a decrease in actual flow across the filter, and (2) the flow reported at standard temperature and pressure was significantly different from the volumetric flow established by the critical orifice across the 47 mm quartz filters used for EC/OC analysis. In order to address the flow problems, a Bios primary flow standard (Mesa Labs, Butler, NJ) was used to measure both volumetric and standard flow rates at the inlet of the AE31 for each of the test conditions, and the reported flow rates were adjusted accordingly. A summary of the flow variability and correction is included in the supporting information. The PAX870, used for diesel engine tests, and the PAX532, used for all solid fuel and small source tests, are integrated nephelometers, quantifying light scattering at a set wavelength, and a photoacoustic absorption monitor, measuring the change of frequency in which particles resonate when heated by an internal light source and quantifying the associated acoustic signal as an absorption coefficient. The PAX measures light absorption without the need for

Table 1. Summary of Emission Source Materials and Combustion Conditions[a]

Emission Source	Test Repeats	Total Aethalometer Measurements	Average EC/TC Ratio	Description
Wood pellet (forced draft)	3	12	0.653	hardwood blend pellets (Indeck Pellets, Ladysmith, WI) in a custom-built stove with forced draft; closed chamber dilution
Kerosene lamp	2	22	0.201	reagent grade kerosene (Sigma-Aldrich Co.) in a flat wick lantern; closed chamber dilution
Diesel engine idle (Diesel 1)	3	21	0.289	Cummins 2010 heavy-duty engine operated at steady state, hot start, 650 rpm, 10% load, 128°C exhaust temperature; constant volume sampler (CVS) tunnel; operated with diesel oxidation catalyst (DOC) and exhaust gas recirculation (EGR).
Lignite coal	3	26	0.027	Lignite (Energy and Environmental Research Center, Grand Forks, ND) coal in a cast iron, box stove with natural draft, 63,801 BTU capacity; CVS hood
Peat	3	28	0.023	peat briquettes (Ireland Earth) in a cast iron, box stove with natural draft, 63,801 BTU capacity; CVS hood.
Leaf litter	3	32	0.032	hardwood leaf litter, silver maple, and black walnut mix, air dried in a cast iron, box stove with natural draft, 63,801 BTU capacity; CVS hood.

[a]Test repeats represent the number of valid repeated tests and total aethalometer readings represent the number of reading collected during all valid test runs. These represent the total number of readings applied to the linear regression slope correction determination. A complete list of sources is reported in the supporting information of this manuscript.

filter media, thus avoiding the interferences associated with filter artifacts. A Radiance Research nephelometer was used to measure scattering independent of the PAX. The nephelometer was adapted for source testing by sealing the unit with Teflon tape and replacing the stock flow control fan with critical orifice flow control.

2.5. Combustion Fuels

A range of fuels were selected based on availability and representativeness. The fuels represent both biomass and fossil fuels that are likely to be used in a combustion setting that would not necessarily incorporate additional emission controls and thus give insight to real-world sources. The heavy-duty diesel engine used standard on-highway fuel with a cetane number of 47.4, density of 845.0 kg m^{-3}, and sulfur content of 6 ppm. Nondiesel fuels were generally obtained from commercial sources, including kerosene, pelletized biomass, peat briquettes, and low-quality coals. Leaf litter was collected directly from an urban forest setting and prepared by air drying outdoors. Table 1 and Table S2 in the supporting information list the specific fuel type used during testing along with a brief description of the combustion conditions and number of replicate measurements for each fuel type.

3. Theory/Calculation

3.1. Aethalometer Correction

Filter-based absorption methods are known to exhibit measurement artifacts associated with the filter substrate, aerosol scattering, and filter loading [*Coen et al.*, 2010; *Jimenez et al.*, 2007]. The applied correction method assumes that major changes in the aerosol composition do not occur over the averaging period for both scattering and absorption measurements. In order to meet these requirements, near-steady state combustion conditions were maintained during testing. A multiple-linear regression correction technique was applied to all results to address source- and wavelength-specific measurement artifacts. This method allows for AE31 correction independent of the single wavelength photoacoustic results, which are not representative of light absorption across the seven discrete wavelengths reported by the AE31. To apply the correction, the AE31 wavelength-specific black carbon (BC_{AE31}, $ng^1\,m^{-3}$) concentration at time (t) of the sample event was multiplied by the aethalometer internally set specific attenuation value $\alpha_{AE31,\lambda}$.

Table 1 shows the summary of emission source materials and combustion conditions. Test repeats represents the number of valid repeated tests, and total aethalometer readings represent the number of reading collected during all valid test runs. These represent the total number of readings applied to the linear regression slope correction determination. A complete list of sources is reported in the supporting information of this manuscript in which $\alpha_{AE31,\lambda} = 14625/\lambda$ ($m^2\,g^{-1}$), where λ is the wavelength in nanometer in order to obtain the uncorrected absorption coefficient $\sigma_{AE31,\lambda}$ (Mm^{-1}) as follows:

$$\sigma_{AE31,\lambda(t)} = BC_{\sigma_{AE31,\lambda(t)}} \times \alpha_{AE31,\lambda} \div 1000 \quad (1)$$

A loading correction factor is determined by applying a multiple-linear regression function ($y_j = b_0 + b_1x_{1j} + b_2x_{2j}$) to the data set, with $\sigma_{AE31,\lambda,(t)} = y_j$, the dependent variable, and $\sigma_{neph\ scat,(t)} = X_{1j}$ and $ATN_{\lambda,(t)} = X_{2j}$, the independent variables. Here $\sigma_{neph\ scat,(t)}$ is the average scattering measured by the nephelometer at time (t) of the test, and $ATN_{\lambda,(t)}$ is the aethalometer wavelength-specific total attenuation since the advancement of the tape at time (t) of the test. Using the Microsoft Excel® linear regression function, the regression coefficient (b) for each of the independent variables was calculated. Here b_0 is the intercept of regression function, b_1x_{1j} represents the fluctuation of PM concentration as indicated by the measured scattering, and $b_2 = b_{ATN} = M_{ATN}$ is the best fit slope as a function of the ATN. The calculated $b_{ATN,\lambda} \times ATN_{\lambda,(t)}$ represents the filter loading artifact at time (t) of the test. The source-specific slope correction values and the associated level of confidence (P values) are reported in Table S1 in the supporting information). In this research, the P value was not used as criteria for application of the slope correction but is reported as an indicator of the slope value suitability of fit. However, poor fit does not necessarily indicate a correction bias. The reader should make note when $|M|$ is greater than 3 and the P value is greater than 0.10. The calculated loading correction $M_{ATN,\lambda}$ is applied to the measured $\sigma_{AE31,\lambda,(t)}$ in the following manner:

$$\sigma_{ldcor,\lambda,(t)} = \sigma_{AE31,\lambda,(t)} + M_{ATN,\lambda} \times \left(ATN_{ref,\lambda} - ATN_{\lambda,(t)}\right) \quad (2)$$

Here $\sigma_{ldcor,\lambda,(t)}$ is the loading-corrected absorption coefficient at time (t) of the test. $ATN_{ref,\lambda,}$ is the first valid ATN value, typically the second aethalometer measurement. On several of the tests, the first data point collected by the AE31 would exhibit a high degree of variation across the seven different channels, resulting from measurement channels changing as sample was introduced into the manifold, replacing pure dilution air. This data point was omitted from the correction methodology as it was not representative of the source. This slope function is similar to that applied by Park et al. and Virkkula et al., as well as the new Magee Scientific AE33 with an internal loading correction, with the primary difference in derivation; these methods use internal absorption measurements as the explanatory variable to derive the ATN slope correction, while the method here uses an independent scattering measurement as the explanatory variable for slope derivation [*Drinovec et al.*, 2014; *Park et al.*, 2010; *Virkkula et al.*, 2007]. It should be noted that $M_{ATN,\lambda}$ is typically negative, leading to a positive correction as the total ATN increases over time. However, this is not always the case; in some instances, there is no significant net change to the aethalometer-reported values; and on other occasions, a negative correction was applied to the aethalometer raw results. Finally, the loading-corrected value was corrected for wavelength-specific multiple scattering resulting from nonabsorbing aerosol similar to the empirical method reported by Bond et al. for the PSAP [*Bond et al.*, 1999a]. A linear correction value was obtained for each of the aethalometer's seven wavelengths by comparing the absorption of multiple-suspended sodium chloride and sodium sulfate concentrations to scattering measured by the nephelometer. These salts have similar real refractive index (RI) of 1.55 and 1.48, respectively, as RI commonly used in climate models to represent organic aerosol scattering. In addition, the correction functions were developed with particle size ranges similar to the tested source samples [*Freedman et al.*, 2009; *Haynes and Lide*, 2011; *Toon et al.*, 1976]. The supporting information to this manuscript includes a summary of the nonabsorbing aerosol results. The scattering correction was applied in the following manner:

$$\sigma_{cor,\lambda,(t)} = \sigma_{ldcor,\lambda,(t)} - m'_{\lambda} \times \sigma_{Neph\ \ scat,(t)} \quad (3)$$

Here $\sigma_{cor,\lambda,(t)}$ is the loading and scattering-corrected wavelength-specific absorption coefficient, and m'_{λ} is the scattering correction factor determined by the linear regression of the nonabsorbing aerosol absorption and nepthalometer scattering. Finally, $\sigma_{cor,\lambda,(t)}$ was averaged over the sampling period to determine the individual emission test absorption coefficient, $\sigma_{source,\lambda}$. It should be noted that an additional correction associated with

the multiple light scatter within the filter is often applied when correcting aethalometer data; we have applied this correction as a final step when reporting the MAC for sources. The results section documents the nonfilter-based PAX absorption measurements with the corresponding corrected aethalometer measurement, $\sigma_{source,\lambda}$, which describes the relationship between the filter and nonfilter-based measurements. Additional discussion of these measurements follows in the results section.

3.2. Segregation of Black and Brown Carbon

The contribution of black carbon and brown carbon to the total bulk absorption coefficient of the emission source is segregated by projecting the absorption at higher wavelengths, 880 nm in this research, to lower wavelengths of the spectrum measured by the aethalometer. The absorption at the higher wavelength is assumed to be attributed to only BC absorption, while absorption at lower wavelengths is attributed to both BC and BrC. The simple extrapolation method using an AAE has been used in several studies and is described in detail by *Lack and Langridge* [2013] [*Ajtai et al*., 2011; *Bahadur et al*., 2012; *Cazorla et al*., 2013; *Chung et al*., 2012a; *Esposito et al*., 2012; *Favez et al*., 2009; *Fialho et al*., 2005; *Lack and Langridge*, 2013; *Massabo et al*., 2013; *Sandradewi et al*., 2008a]. Although *Lack and Langridge* [2013] note significant uncertainties using this method, in particular when the BrC component of absorption is relatively small compared to the BC absorption, directly applying this method to sources which have high BrC components and effectively applying emission test-specific corrections to the aethalometer results shows that this method is an effective way to estimate the BrC absorption. The AAE is calculated as shown in equation (4). This equation is used to calculate the AAE and project the corrected aethalometer results to equivalent PAX wavelengths of 532 nm and 870 nm using the neighboring absorption coefficients. It also is used to project the absorption coefficient at 880 nm to the other aethalometer wavelengths using an AAE = 1, to estimate the BC contribution of the bulk absorption coefficient. Using the AAE = 1 projection, the BC component $\sigma_{BC,AAE=1,\lambda}$ of the bulk absorption coefficient can be calculated for each wavelength of interest; subtracting this value from the bulk absorption coefficient $\sigma_{source,\lambda}$ results in the net BrC absorption coefficient, $\sigma_{BrC,\lambda}$ as shown in equation (5).

$$AAE = -\frac{\ln\left(\frac{\sigma_{cor,\lambda 1}}{\sigma_{cor,\lambda 2}}\right)}{\ln\left(\frac{\lambda_1}{\lambda_2}\right)} \tag{4}$$

$$\sigma_{BrC,\lambda} = \sigma_{source,\lambda} - \sigma_{BC,AAE=1,\lambda} \tag{5}$$

3.3. Mass Absorption Cross Section

In order to understand the BC and BrC absorption contributions from each source, the MAC is calculated at each corresponding AE31 wavelength. The bulk EC MAC ($MAC_{EC,\lambda}$) is calculated by dividing the $\sigma_{source,\lambda}$ by the EC filter concentration; the BC projected MAC ($MAC_{BC,\ AAE=1,EC,\lambda}$) is calculated by dividing the $\sigma_{BC,\ AAE=1,\ \lambda}$ by the EC filter concentration; and the BrC MAC ($MAC_{BrC,OC,\lambda}$) is calculated by dividing $\sigma_{BrC,\lambda}$ by the OC filter-based concentration. In order account for filter scattering artifact, the MAC values are divided by the PAX/AE31 slope value (average of the 532 and 870 slopes = 5.92) discussed below.

4. Results

It should be noted that the absorption coefficient can vary greatly under changing combustion conditions. This is due to the fact that absorption intensity will change with combustion emission rates, system dilution, and particle composition. During the sampling, dilution was maintained to allow particle aging, sufficient sample collection time before the AE31 automatic tape advance, and adequate mass loading for EC/OC analysis. Absorption coefficients offer insight on the repeatability and representativeness of the measurement as shown in Figures 1a and 1b. These figures show good correlation between the $PAX_{532/870}$ under both varied composition and concentrations ($R^2 = 0.851$ at 532 nm; $R^2 = 0.961$ at 870 nm). Figure 1a shows the corrected AE31 versus the PAX_{532} at a wavelength of 532 nm. The AE31 values are estimated at 532 nm using a calculated AAE from $\sigma_{source,520}$ and $\sigma_{source,590}$. The linear regression of both the corrected and not corrected are shown. While the multiple-linear regression correction method can have a significant single reading correction on $\sigma_{Idcor,\lambda,(t)}$, as time passes during source testing, in general, at 532 nm for near-steady state combustion conditions, the average $\sigma_{source,\lambda,}$

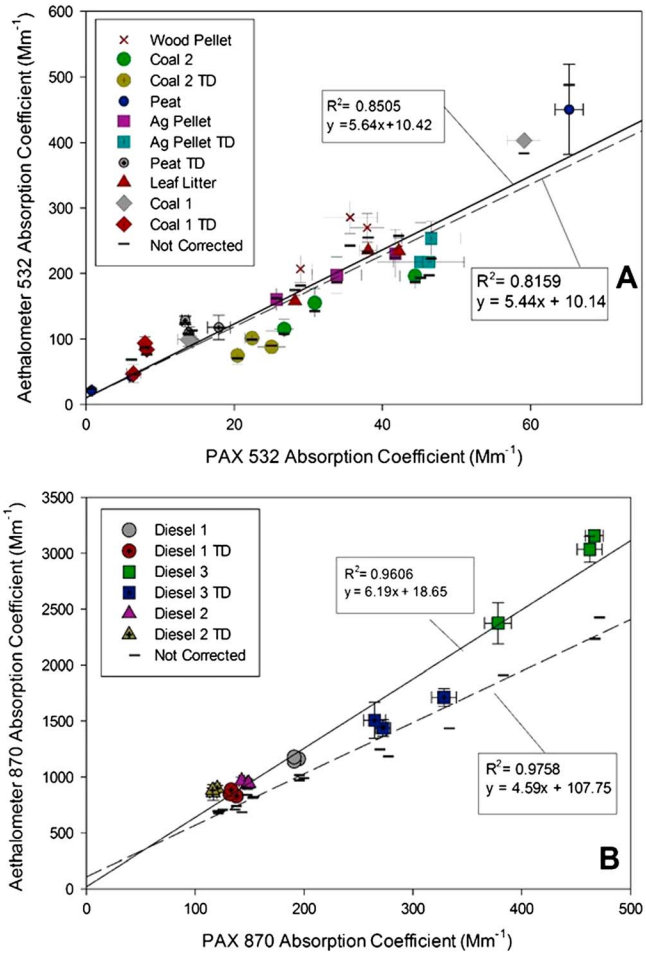

Figure 1. Comparison of filter-based AE31 results to PAX photoacoustic absorption results. Results have been corrected for wavelength-specific filter loading and multiple scattering but have not been normalized to the PAX absorption measurements represented by the regression line slope. The slope is an indicator of the filter enhancement associated with the filter-based AE31 measurements. (a) The absorption coefficient (Mm^{-1}) of biomass and coal reported by the PAX532 and corrected AE31 values projected with AAE determined by neighboring absorption coefficients. Corresponding uncorrected AE31 values are shown as a hash marks. (b) The absorption coefficient (Mm^{-1}) of diesel emissions reported by the PAX870 and corrected AE31 values projected with AAE determined by neighboring absorption coefficients.

did not change significantly. The limited impact from the regression correction is a result of the relative sensitivity at the wavelength of interest, averaging across the time base, and the fact that the scattering correction tends to decrease the test average absorption while the loading correction tends to increase the test average absorption. Figure 1b shows the corrected AE31 versus the PAX_{870} at a wavelength of 870 nm, with the AE31 projected to wavelength of 870 nm using the AAE method with $\sigma_{source,660}$ and $\sigma_{source,880}$. While both the corrected and noncorrected correlate with the PAX_{870} based on the R^2 value, the correction resulted in a significant shift in the regression line slope and a *y* intercept that is significantly closer to the origin. The PAX_{870} was only available during diesel engine testing, where the emissions exhibited an insignificant $\sigma_{neph\ scat,(t)}$ during the testing; thus, the correction is dominated by the filter loading correction. Here the correction methodology can have a significant impact on AE31 values, especially tests that are run at lower dilution ratios. The linear regression slope values for the corrected results are 5.64 and 6.19, representing the values required to correct the AE31 absorption coefficients to PAX absorption coefficients at 532 and 870 nm, respectively. In this manuscript we do not implement the final correction step except for when reporting the MAC that is derived by normalization to a mass concentration. In theory, applying the PAX/aethalometer ratio accounts for multiple scattering in the filter media, and while the PAX values are filter artifact free, the reported PAX absorption is still a function of the instrument calibration, thus not necessarily an absolute value. Regardless, the measured absorption coefficients correlate well using two independent methods and thus indicate the robustness of the AE31-reported values. The reported results have similar ratios (in this study average of 5.92) to other studies that measured both photoacoustic and aethalometer light absorption. Estimating the slope from photoacoustic versus aethalometer data reported by Arnott et al. for ambient and Kamboures et al. for gasoline vehicles, a range of 3 and 6.9 to 7.9, respectively, can be inferred from noncorrected aethalometer data [*Arnott et al.*, 2005; *Kamboures et al.*, 2013]. This estimation assumes that the average BC mass concentration reported by aethalometer was similar across the visible wavelengths of interest.

In order to compare emission sources independent of the variations in dilution, each source type's absorption coefficient was divided by the EC mass concentration as measured at the sample manifold to determine the bulk $MAC_{EC,\ \lambda}$. Table 1 reports the EC to total carbon (TC) ratios for selected source

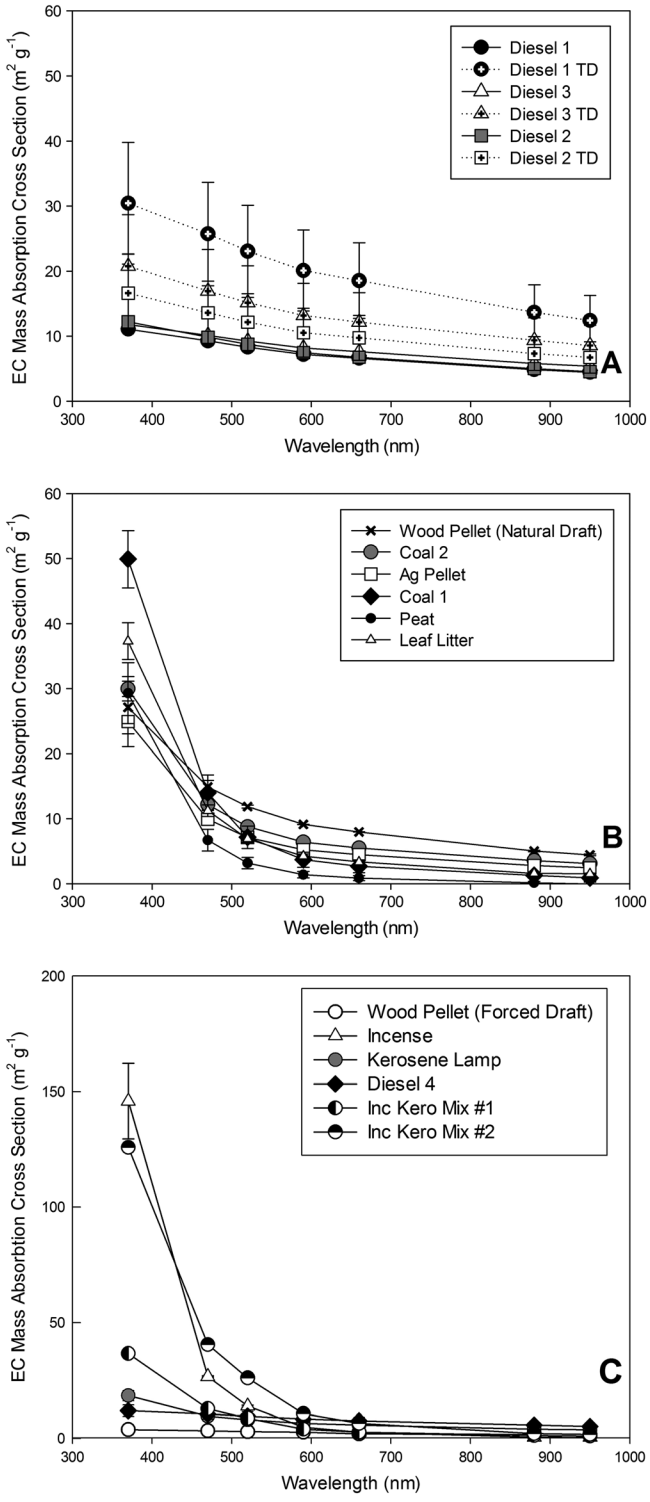

Figure 2. Corrected bulk EC mass absorption cross section for combustion sources. Results have been corrected for wavelength-specific filter loading, multiple scattering, and have been normalized to the PAX/AE31 slope correction. (a) The Bulk EC MAC of diesel emissions, including TD conditioned emissions which demonstrated excessive EC particle loss. (b) Biomass and coal EC MAC. (c) The EC MAC of multiple material types showing the sensitivity of visible light absorption as function of different source types and compositions.

emissions, and all samples EC/OC results are reported in the supporting information. The EC/TC range from 0.65 for wood pellets with forced air mixing to 0.023 for peat briquettes. This demonstrates the carbonaceous composition sensitivity due to combustion conditions and fuel types, indicating the need for proper understanding of source composition in order to interpret absorption measurements, in particular, the OC contribution to BrC. Figure 2 shows the bulk $MAC_{EC,\ \lambda}$ for multiple-source types and TD conditions. Figure 2a details the absorption spectra of diesel engine emission, with error bars representing the standard error between repeated test conditions. The results indicate that individual test runs under the same conditions are very repeatable; however, there is an observable shift when test conditions (e.g., engine speed and TD temperature) are changed for the same emission source. The shift in MAC profiles is a function of multiple known factors that can result in uncertainty associated with measured value. The NIOSH 5040 method has known variability among diesel samples depending on OC content and loading, and the mixing state and morphology are important contributors to particle scattering and absorption [*China et al.*, 2015; *Khan et al.*, 2012]. Changes in engine mode and after treatment can heavily impact both OC content and particle morphology [*Lapuerta et al.*, 2009]. The aerosol OC fraction's impact on MAC is further discussed later in the manuscript. Diesel emissions with reduced OC content, due to the application of a diesel oxidative catalysis (DOC) which removes OC from the emissions as part of the after treatment, did not show a quantifiable BrC component. Applying an exponential least squares fit to the corrected absorption coefficients for this test condition resulted in an AAE value of 1.053 ± 0.006 for the diesel engine conditions with significant EC content. As discussed previously, an AAE of one is typical for aerosols consisting of primarily BC. It should be noted that data not reported

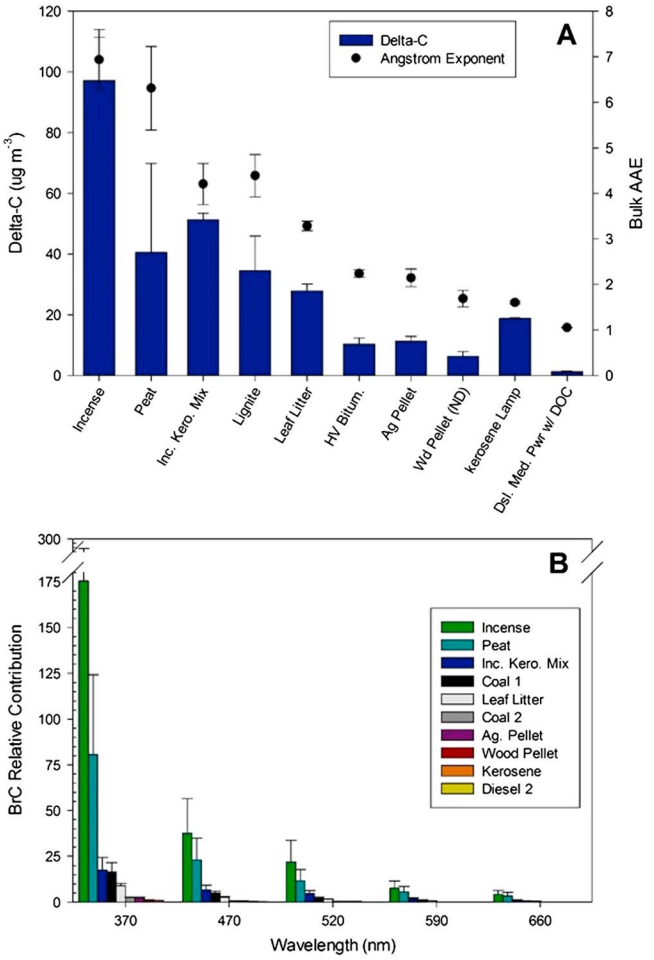

Figure 3. (a) The calculated Delta C and AAE for various emission sources. (b) The relative BrC contribution ($\sigma_{BrC,\lambda}/\sigma_{BC,AAE=1,\lambda}$) of various source emissions. Results indicate high variability of absorption across sources.

in this manuscript but detailed in a publication by *Robinson et al.*, 2015 show that diesel emissions can result in significant absorption at the UV wavelengths, resulting in an AAE greater than one, when emissions consist of very high OC fractions observed at idle speed with no after treatment controls [*Robinson et al.*, 2015].

Solid fuels tested show much more variability in the absorption spectra as compared to diesel engine emissions. Figure 2b shows the emission from contained solid fuel combustion sources. Woodsmoke emissions are often considered to result in significant UV and near-UV absorption; however, the results show that other sources including lignite and high-volatility bituminous coals exhibit a similar absorption spectrum in the near-UV range. Additionally, the degree in which the absorption measured at 370 nm is representative of absorption in the middle of the visible spectrum can vary significantly. For example, the high absorption by lignite and peat at 370 nm is not observed at 590 and 660 nm wavelengths, while the relative absorption by wood pellet emissions at these wavelengths is significant. The bulk MAC intensity can vary greatly among sources; however, when externally mixed separate source aerosols were created through simultaneous combustion of incense and a kerosene lamp in a closed chamber (note that emission contributions were variable and not equal for each of the sources), the combination was not always a direct averaging across the MAC spectrum. For example, at 370 nm the combination MAC sits between the extremes of the single source emissions of kerosene and incense, and at wavelengths between 470 and 660 nm, the incense-kerosene mix #1 continued to follow this trend. However, the incense-kerosene mix #2 did not follow this trend and in fact showed a greater absorption at the lower wavelengths than emissions from its components. This is a result of the varied absorption intensities of source emissions across the spectrum, but other factors like particle mixing state and aerosol composition creating a lensing effect, enhancing the total absorption by particles at individual wavelengths, are also likely contributors [*Lack et al.*, 2009]. Figure 2c demonstrates both the high degree of variability in source emission absorption properties and the change in optical properties with mixed source emissions.

Methods such as the Delta C (Delta $C = UVBC_{370nm} - BC_{880nm}$ reported by the aethalometer) and AAE calculated by the power law best fit allow a direct assessment of the relative change in absorption across a wide range of the visible spectrum, thus act as indicators of BrC. In this study we applied corrected BC concentrations at 880 nm and 370 nm prior to calculating the Delta C in $\mu g\,m^{-3}$. A Delta C value that is significantly greater than zero indicates the presence of nonrefractory light absorbing carbon, often assumed to be wood burning particles [*Wang et al.*, 2011]. Similarly, an Angstrom exponent greater than one, the value often attributed to PM dominated by a BC composition, also indicates the presence of other light absorbing PM components [*Russell et al.*, 2010]. These methods do not, however, quantify the overall structure of the absorption spectrum, especially in the context of changes associated with different emission

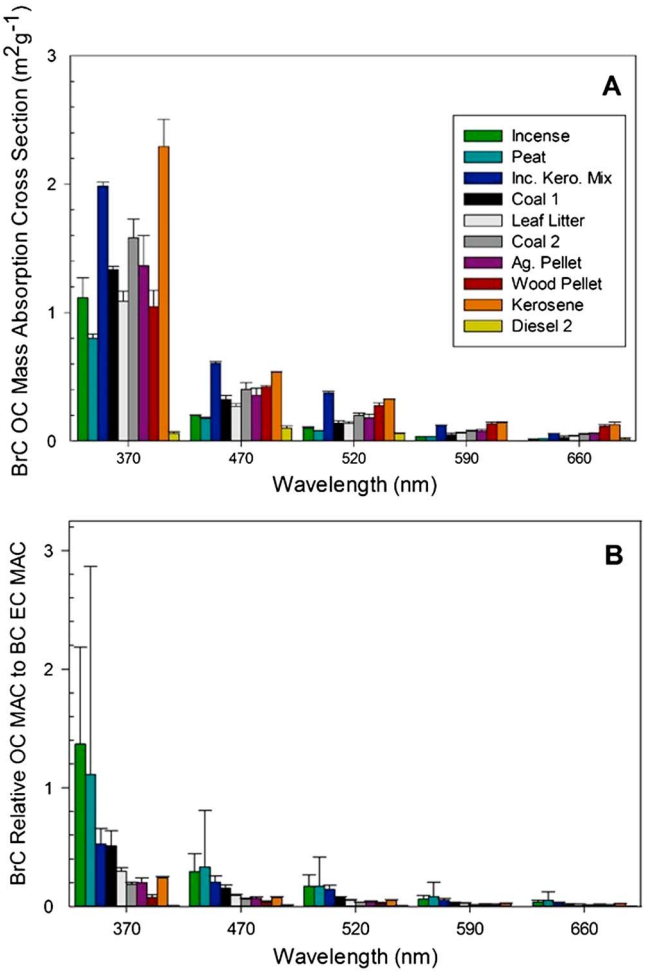

Figure 4. (a) Brown carbon $MAC_{BrC,OC,\lambda}$ for selected sources showing the relative strength of OC light absorption at multiple wavelengths. (b) The relative strength of BrC absorption ($MAC_{BrC,OC,\lambda}/MAC_{BC,\ AAE=1,EC,\lambda}$) as compared to BC absorption at multiple wavelengths. MAC filter correction includes PAX to AE31 average slope value from Figure 1.

sources. Additionally, it is suggested that Delta C and AAE may be good indicators of biomass emissions; however, other sources such as lignite and kerosene can demonstrate high Delta C and AAE values. Figure 3a reports these values for selected emission sources calculated based on the $\sigma_{source,\lambda}$. Figure 3b shows the BrC relative contribution of absorption, ($\sigma_{BrC,\lambda}/\sigma_{BC,AAE=1,\ \lambda}$) as compared to the BC contribution calculated using an AAE = 1 projection to better understand the structure of the absorption spectrum profile and the sensitivity that source emissions have across the visible wavelengths. As indicated in Figure 3b, incense and peat emissions display extremely high absorption at 370 nm, 175 and 80 times (respectively) higher than their BC contribution; error bars represent the standard error between repeated tests. However, these sources' relative BrC contribution of absorption compared to the BC component is only 22 and 12 times, respectively, at the 520 nm wavelength. This indicates that caution needs to be taken when using UV absorption to infer the absorption across visible wavelengths. Other source emissions demonstrated a weaker BrC absorption component across the visible wavelengths, and in general the BrC component disappeared at the 660 nm wavelength and higher. This analysis is useful to understand a source test's absorption spectrum characteristics, but in order to understand the relative absorptive strength of the OC component from individual sources, a comparison of $MAC_{BrC,OC,\lambda}$ is required. The comparison of the relative OC contribution to BrC from multiple-emission sources is detailed in Figure 4a. These results show that the OC concentration of the emission can have a significant impact on the absorption measurement. There is notable variation in absorption across source types; the $MAC_{BrC,OC,\lambda}$ does not exhibit the same extremes as the $\sigma_{BrC,\lambda}$. When the OC concentration is accounted for, the incense and peat emissions are not the strongest absorbers at 370 nm ($1.11 \pm 0.15\ m^2\ g^{-1}$ and $0.8 \pm 0.03\ m^2\ g^{-1}$, respectively) but rather kerosene ($2.29 \pm 0.21\ m^2\ g^{-1}$) shows the strongest absorption, and all emission sources, with the exception of a diesel engine, show a quantifiable BrC absorption across all wavelengths. For example, the $MAC_{BrC,OC,590}$ ranged from $0.03 \pm 0.004\ m^2\ g^{-1}$ for incense to $0.14 \pm 0.004\ m^2\ g^{-1}$ for kerosene lamp emissions. Table 2 (with the remainder of emission values reported in the supporting information) summarizes a selected set of source emission $MAC_{BrC,OC,\lambda}$, showing the wavelength-specific BrC strength from several of the sources along with the $MAC_{BC,\ AAE=1,EC,\lambda}$. The results indicate the varying degree of BrC absorption from sources and show that the BC across the visible spectrum dominates the absorption from sources; however, if significant OC is present, BrC can become a major contributor to UV and near-UV absorption. Negative $MAC_{BrC,OC,\lambda}$ results indicate that the actual AAE for the $\sigma_{source,\lambda}$ was less than one, as reported for a diesel engine at high power output. Figure 4b shows wavelength-specific relative contribution of BrC MAC ($MAC_{BrC,OC,\lambda}/MAC_{BC,\ AAE=1,EC,\lambda}$) to BC absorption with error bars representing the standard error between repeated source test results. Here it is clear

Table 2. A Summary of Selected Mass Absorption Cross Sections (MAC) Demonstrating the Variability of Source Emissions Absorption Properties and the Relative Importance of BrC Absorption for Sources

		370 nm		470 nm		520 nm		590 nm		660 nm		880 nm	
Emission source		m^2/g	SE	m^2/g	SE	m^2/g	SE	m^2/g	SE	m^2/g	SE	m^2/g	SE
Wood	Bulk MAC_{EC}	4.52	±0.33	3.73	±0.3	3.34	±0.28	2.87	±0.28	2.66	±0.32	1.92	±0.21
Pellet	$BC_{Å=1}$ MAC_{EC}	4.58	±0.87	3.6	±0.69	3.26	±0.62	2.87	±0.55	2.57	±0.49	1.92	±0.36
(Forced draft)	BrC MAC_{OC}	0.21	±0.16	0.42	±0.17	0.3	±0.12	0.07	±0.08	0.13	±0.04	0.00	±0.00
	Bulk MAC_{EC}	49.91	±4.38	14	±2.72	7.15	±1.72	3.68	±1.15	2.69	±0.97	1.01	±0.56
Coal 1 (Lignite)	$BC_{Å=1}$ MAC_{EC}	2.4	±1.34	2.42	±1.27	1.71	±0.95	1.51	±0.84	1.34	±0.75	1.01	±0.56
	BrC MAC_{OC}	1.35	±0.01	0.32	±0.05	0.15	±0.01	0.06	±0.00	0.03	±0.00	0.0	±0.00
	Bulk MAC_{EC}	29.31	±4.7	6.7	±1.67	3.15	±0.87	1.38	±0.48	0.86	±0.39	0.14	±0.23
Peat	$BC_{Å=1}$ MAC_{EC}	0.33	±0.55	0.26	±0.75	0.23	±0.39	0.21	±0.34	0.18	±0.3	0.14	±0.23
	BrC MAC_{OC}	0.8	±0.03	0.17	±0.01	0.07	±0.00	0.03	±0.00	0.01	±0.00	0.0	±0.00
	Bulk MAC_{EC}	37.33	±2.82	11.24	±0.9	6.9	±0.55	4.26	±0.32	3.34	±0.23	1.58	±0.12
Leaf litter	$BC_{Å=1}$ MAC_{EC}	3.76	±0.3	2.96	±0.41	2.67	±0.21	2.36	±0.18	2.1	±0.16	1.58	±0.12
	BrC MAC_{OC}	1.08	±0.07	0.26	±0.04	0.13	±0.01	0.06	±0.00	0.04	±0.00	0.0	±0.00
Diesel 1	Bulk MAC_{EC}	11.07	±0.08	9.28	±0.06	8.3	±0.06	7.18	±0.06	6.61	±0.05	4.86	±0.05
(Idle DOC, EGR)	$BC_{Å=1}$ MAC_{EC}	11.57	±0.12	9.11	±0.09	8.23	±0.08	7.25	±0.07	6.48	±0.06	4.86	±0.05
	BrC MAC_{OC}	−0.23	±0.06	0.07	±0.00	0.02	±0.00	−0.03	±0.01	0.05	±0.00	0.0	±0.00
	Bulk MAC_{EC}	18.41	±2.24	9.54	±1.06	8.17	±0.92	6.5	±0.86	5.81	±0.81	3.98	±0.54
Kerosene	$BC_{Å=1}$ MAC_{EC}	9.65	±1.33	7.6	±1.05	6.87	±0.94	6.06	±0.83	5.42	±0.74	4.05	±0.56
	BrC MAC_{OC}	2.29	±0.21	0.53	±0.00	0.32	±0.00	0.14	±0.00	0.12	±0.02	0.0	±0.00

that UV absorption can be dominated by BrC, especially for incense, peat, and lignite sources with significantly high OC concentrations. These source emissions, along with others tested, could result in BrC dominating the overall absorption at wavelengths less than 470 and 520 nm.

In order to further understand the effect of an aerosol's EC/OC composition on measured absorption, a best fit spline curve was applied to all of the individual emission results. MATLAB R2014a was used to apply smooth curves to the set of bulk $MAC_{EC,\lambda}$ versus the OC fraction (OC/TC) using the smoothing spline fit type, with normalization on and a smoothing parameter set to 0.5 for all wavelengths. Figures 5a and 5b show the fit curve applied to the 370 and 880 nm wavelengths, and Figure 5c shows all of the curve results from 370 to 880 nm. The low-wavelength curves show increased absorption with increased OC content even as the emissions, and thus chemical composition, vary significantly among sources [*Schauer et al.*, 1996]. As discussed previously, the bulk MAC is variable for each source emission, and the overall sensitivity to the changing emission types can be assessed by comparing the R^2 value for the fitted curve at each wavelength. The R^2 at 370 and 880 nm wavelengths show the least amount of variability when fit to all of the emission source results ($R^2 = 0.531$ and $R^2 = 0.447$, respectively). However, R^2 values for the fit curves at wavelengths 520, 590, and 660 nm were lower: 0.107, 0.072, and 0.183, respectively. This indicates that the absorption values measured at 370 and 880 nm are not always good indicators of the absorption in the central segment of the visible spectrum. In addition, while the curve fit shows better agreement at 880 nm, as OC fraction increases, the amount of absorption decreases significantly. This is partially a result of a known increase in EC uncertainty with increased pyrolysis of OC associated with the NIOSH 5040 method [*Dutton et al.*, 2009]. However, this is unlikely to be the only cause of this observed result. While OC lensing can result in increased absorption, it appears that when a significant portion of the aerosols is composed of OC, the BC absorption is inhibited at higher wavelengths. Core/shell Mie theory has been used to investigate absorption sensitivity to clear and brown carbon coatings and demonstrated a reduction in enhancement with increased carbon content; however, this was predominately at near-UV wavelengths [*Lack and Cappa*, 2010]. The mixing state of aerosols has also been shown to have an impact on the absorption enhancement, with internally mixed, coated particles demonstrating higher MAC than externally mixed aerosols [*Wang et al.*, 2014]. Finally, morphology of biomass combustion can vary significantly from a single source; this morphology directly impacts the absorption properties of individual particles [*Bond and Bergstrom*, 2006; *China et al.*, 2013]. The combination of these factors can result in significant divergence from a typical MAC at higher wavelengths for source emissions.

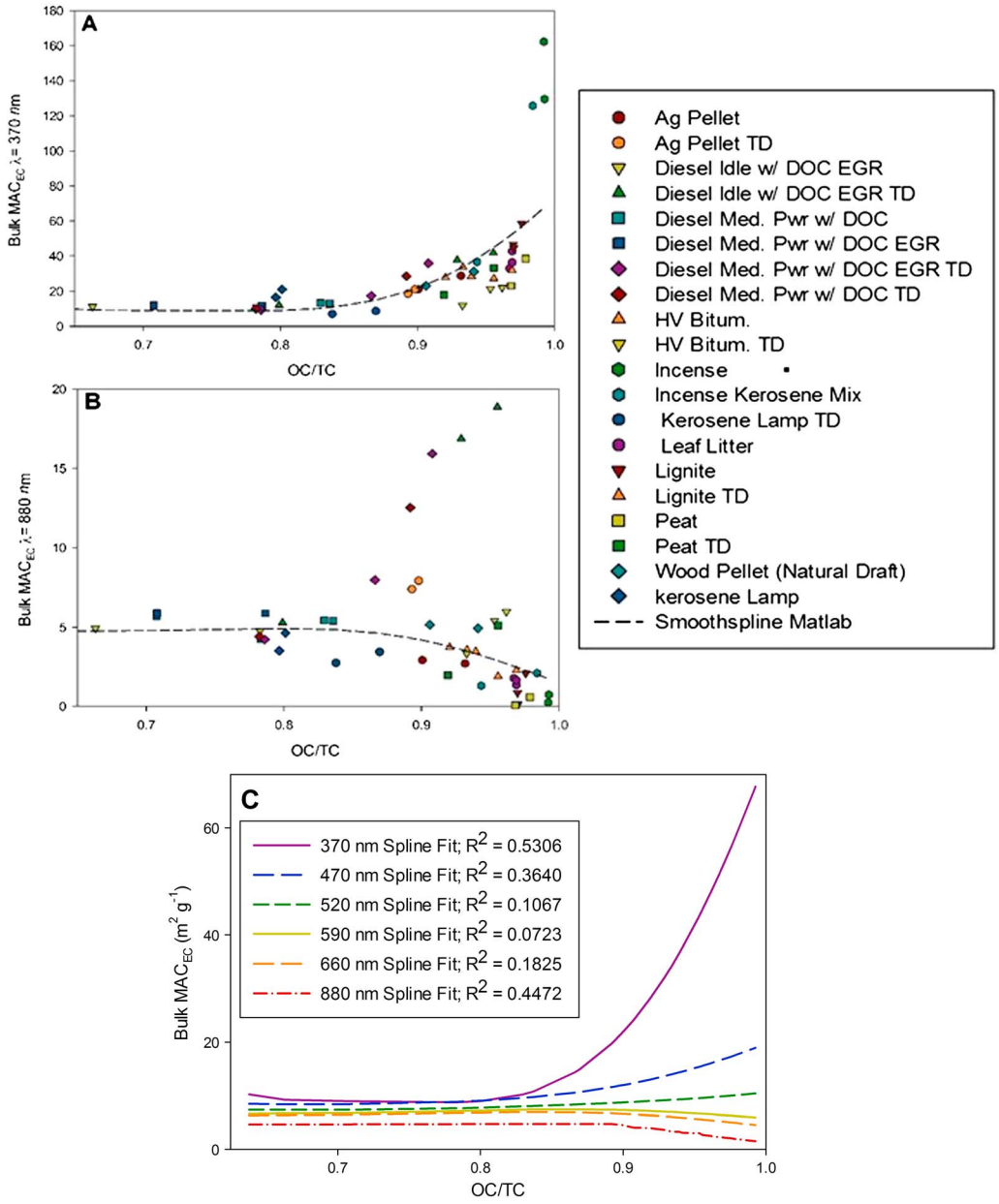

Figure 5. (a) The smoothing splinefit curve applied to $MAC_{EC,\lambda}$ at 370 nm wavelength for all corrected test values. (b) The smoothing splinefit curve applied to $MAC_{EC,\lambda}$ at 880 nm wavelength for all corrected test values. (c) A summary of all wavelength spline curve fits. Curve fit show higher variability at the central wavelengths of visible light.

5. Conclusions

In this research we investigate the light absorption properties of a number atmospherically relevant source emissions. Emissions were measured under controlled conditions allowing for the independent quantification of single source optical properties. Filter-based data were corrected using a wavelength- and test-specific multiple-linear-regression method, and results were corroborated through independent photoacoustic absorption methods. Using an established method of segregating BC and BrC absorption components, we investigate the multiple-wavelength absorption characteristics from individual sources. The overall absorption intensity was highly impacted by the OC content of the emissions, up to 175 times the BC absorption at 370 nm but less than 4.2 times at 660 nm. Source emissions $MAC_{BrC,OC,\lambda}$ and bulk $MAC_{EC,\lambda}$ were compared allowing an evaluation of individual combustion source emission's ability to absorb visible light.

Nonwoodsmoke sources, such as kerosene and soft coals, can have significant BrC absorption contribution, manifested in the bulk $MAC_{EC,\lambda}$ at lower wavelengths when relatively high levels of OC (>0.9 OC/TC) are present in the emission. This indicates that caution needs to be taken when interpreting multiple-wavelength indicators of BrC, such as Delta C and high AAE, to estimate source contributions. This observation may be a particular concern in areas where both uncontrolled coal and biomass combustion occurs.

Corrected filter-based absorption measurements at multiple wavelengths agreed well with nonfilter-based photoacoustic measurements when averaged over a source sampling event. It should be noted that the corrections did not have a large impact on final emission result interpretation, as the measurements were averaged throughout the entire test run and scattering and loading artifact correction components tended to offset one and another; however, filter scattering correction was substantial, with an average multiplier of 5.92 for the 532 and 870 wavelengths compared in this study. When looking at individual time series data points, the loading correction can become very important, and caution needs to be taken when running dynamic emission tests. As is, source testing in a controlled environment allows for the effective segregation of the BC and BrC components of emissions. The $MAC_{BrC,OC,\lambda}$ (maximum reported of $2.29\,m^2\,g^{-1}$ for Kerosene at 370 nm) and bulk $MAC_{EC,\lambda}$ (ave. at $520\,nm = 9.0 \pm 3.7\,m^2\,g^{-1}$; with OC fraction $< 0.85 = \sim 7.5\,m^2\,g^{-1}$) reported in this manuscript can be applied to source apportionment models to reconstruct observed optical measurements and be applied to climate models to more accurately predict source emission impacts on climate forcing.

Acknowledgments

This publication was made possible by U.S. EPA grant (R835039). Its contents are solely the responsibility of the grantee and do not necessarily represent the official views of the U.S. EPA. Further, U.S. EPA does not endorse the purchase of any commercial products or services mentioned in the publication. In addition, we would like to thank the following individuals and entities for their support of this research: Cummins Emission Solutions, Stoughton WI; USDA Forest Products Research Laboratory, Madison, WI; Wisconsin State Laboratory of Hygiene, Madison, WI, for chemical analysis support; Ken Ragland UW-Madison Professor Emeritus for expertise in solid fuel combustion, Charles Boardman USFS for sampling support; and the following UW-System graduate and undergraduate researchers: Charlie Feit, Jerome McGinnis, Ying Zhan, Austin Yantes, Jongbae Heo, Kristin Short, and Rebecca Goldberg. Data used to develop the figures and addition results not specifically discussed in the manuscript are reported in the supporting information. All results reported in this paper are available to readers at the NERSC repository http://www.nersc.gov/users/science-gateways/.

References

Ajtai, T., A. Filep, N. Utry, M. Schnaiter, C. Linke, Z. Bozoki, G. Szabo, and T. Leisner (2011), Intercomparison of optical absorption coefficients of atmospheric aerosols determined by a multiwavelength photoacoustic spectrometer and an aethalometer under suburban wintry conditions, *J. Aerosol Sci.*, *42*(12), 859–866, doi:10.1016/j.jaerosci.2011.07.008.

Anderson, T. L., et al. (1996), Performance characteristics of a high-sensitivity, three-wavelength, total scatter/backscatter nephelometer, *J. Atmos. Oceanic Technol.*, *13*(5), 967–986, doi:10.1175/1520-0426(1996)013<0967:pcoahs>2.0.co;2.

Andreae, M. O., and A. Gelencser (2006), Black carbon or brown carbon? The nature of light-absorbing carbonaceous aerosols, *Atmos. Chem. Phys.*, *6*, 3131–3148.

Arnott, W. P., H. Moosmuller, C. F. Rogers, T. F. Jin, and R. Bruch (1999), Photoacoustic spectrometer for measuring light absorption by aerosol: Instrument description, *Atmos. Environ.*, *33*(17), 2845–2852.

Arnott, W. P., K. Hamasha, H. Moosmuller, P. J. Sheridan, and J. A. Ogren (2005), Towards aerosol light-absorption measurements with a 7-wavelength aethalometer: Evaluation with a photoacoustic instrument and 3-wavelength nephelometer, *Aerosol Sci. Technol.*, *39*(1), 17–29, doi:10.1080/027868290901972.

Bahadur, R., P. S. Praveen, Y. Xu, and V. Ramanathan (2012), Solar absorption by elemental and brown carbon determined from spectral observations, *Proc. Natl. Acad. Sci. U.S.A.*, *109*(43), 17,366–17,371, doi:10.1073/pnas.1205910109.

Bergin, M. H., S. N. Tripathi, J. J. Devi, T. Gupta, M. McKenzie, K. S. Rana, M. M. Shafer, A. M. Villalobos, and J. J. Schauer (2015), The discoloration of the Taj Mahal due to particulate carbon and dust deposition, *Environ. Sci. Technol.*, *49*(2), 808–812, doi:10.1021/es504005q.

Bond, T. C., and R. W. Bergstrom (2006), Light absorption by carbonaceous particles: An investigative review, *Aerosol Sci. Technol.*, *40*(1), 27–67, doi:10.1080/02786820500421521.

Bond, T. C., T. L. Anderson, and D. Campbell (1999a), Calibration and intercomparison of filter-based measurements of visible light absorption by aerosols, *Aerosol Sci. Technol.*, *30*(6), 582–600, doi:10.1080/027868299304435.

Bond, T. C., M. Bussemer, B. Wehner, S. Keller, R. J. Charlson, and J. Heintzenberg (1999b), Light absorption by primary particle emissions from a lignite burning plant, *Environ. Sci. Technol.*, *33*(21), 3887–3891, doi:10.1021/es9810538.

Bond, T. C., D. S. Covert, J. C. Kramlich, T. V. Larson, and R. J. Charlson (2002), Primary particle emissions from residential coal burning: Optical properties and size distributions, *J. Geophys. Res.*, *107*(D21), 8347, doi:10.1029/2001JD000571.

Bond, T. C., et al. (2013), Bounding the role of black carbon in the climate system: A scientific assessment, *J. Geophys. Res. Atmos.*, *118*, 5380–5552, doi:10.1002/jgrd.50171.

Cazorla, A., R. Bahadur, K. J. Suski, J. F. Cahill, D. Chand, B. Schmid, V. Ramanathan, and K. A. Prather (2013), Relating aerosol absorption due to soot, organic carbon, and dust to emission sources determined from in situ chemical measurements, *Atmos. Chem. Phys.*, *13*(18), 9337–9350, doi:10.5194/acp-13-9337-2013.

China, S., C. Mazzoleni, K. Gorkowski, A. C. Aiken, and M. K. Dubey (2013), Morphology and mixing state of individual freshly emitted wildfire carbonaceous particles, *Nat. Commun.*, *4*, doi:10.1038/ncomms3122.

China, S., et al. (2015), Morphology and mixing state of aged soot particles at a remote marine free troposphere site: Implications for optical properties, *Geophys. Res. Lett.*, *42*, 1243–1250, doi:10.1002/2014gl062404.

Chung, C. E., S. W. Kim, M. Lee, S. C. Yoon, and S. Lee (2012a), Carbonaceous aerosol AAE inferred from in situ aerosol measurements at the Gosan ABC super site, and the implications for brown carbon aerosol, *Atmos. Chem. Phys.*, *12*(14), 6173–6184, doi:10.5194/acp-12-6173-2012.

Chung, C. E., V. Ramanathan, and D. Decremer (2012b), Observationally constrained estimates of carbonaceous aerosol radiative forcing, *Proc. Natl. Acad. Sci. U.S.A.*, *109*(29), 11,624–11,629, doi:10.1073/pnas.1203707109.

Coen, M. C., et al. (2010), Minimizing light absorption measurement artifacts of the aethalometer: Evaluation of five correction algorithms, *Atmos. Meas. Tech.*, *3*(2), 457–474.

Drinovec, L., et al. (2014), The "dual-spot" aethalometer: An improved measurement of aerosol black carbon with real-time loading compensation, *Atmos. Meas. Tech. Discuss.*, *7*(9), 10,179–10,220, doi:10.5194/amtd-7-10179-2014.

Dutton, S. J., J. J. Schauer, S. Vedal, and M. P. Hannigan (2009), PM2.5 characterization for time series studies: Pointwise uncertainty estimation and bulk speciation methods applied in Denver, *Atmos. Environ.*, *43*(5), 1136–1146, doi:10.1016/j.atmosenv.2008.10.003.

Esposito, F., M. R. Calvello, E. Gueguen, and G. Pavese (2012), A new algorithm for brown and black carbon identification and organic carbon detection in fine atmospheric aerosols by a multiwavelength aethalometer, *Atmos. Meas. Tech. Discuss.*, *5*(1), 1003–1027, doi:10.5194/amtd-5-1003-2012.

Favez, O., S. C. Alfaro, J. Sciare, H. Cachier, and M. M. Abdelwahab (2009), Ambient measurements of light-absorption by agricultural waste burning organic aerosols, *J. Aerosol Sci.*, *40*(7), 613–620, doi:10.1016/j.jaerosci.2009.04.002.

Feng, Y., V. Ramanathan, and V. Kotamarthi (2013), Brown carbon: A significant atmospheric absorber of solar radiation?, *Atmos. Chem. Phys.*, *13*(17), 8607–8621, doi:10.5194/acp-13-8607-2013.

Feng, Z., et al. (2014), Sensitivity of mesoscale modeling of smoke direct radiative effect to the emission inventory: A case study in northern sub-Saharan African region, *Environ. Res. Lett.*, *9*(7), 075002, doi:10.1088/1748-9326/9/7/075002.

Fialho, P., A. D. A. Hansen, and R. E. Honrath (2005), Absorption coefficients by aerosols in remote areas: A new approach to decouple dust and black carbon absorption coefficients using seven-wavelength aethalometer data, *J. Aerosol Sci.*, *36*(2), 267–282, doi:10.1016/j.jaerosci.2004.09.004.

Freedman, M. A., C. A. Hasenkopf, M. R. Beaver, and M. A. Tolbert (2009), Optical properties of internally mixed aerosol particles composed of dicarboxylic acids and ammonium sulfate, *J. Phys. Chem. A*, *113*(48), 13,584–13,592, doi:10.1021/jp906240y.

Grexa, O., M. A. Dietenberger, and R. H. White (2011), Reaction-to-fire of wood products and other building materials: Part 1, Room/corner test performance *Research Paper - Forest Products Laboratory*, *USDA Forest Service*(FPL-RP-663), i + 49 pp.

Hansen, A. D. A., H. Rosen, and T. Novakov (1984), The aethalometer: An instrument for the real-time measurement of optical-absorption by aerosol-particles, *Sci. Total Environ.*, *36*, 191–196, doi:10.1016/0048-9697(84)90265-1.

Harrison, R. M., D. C. S. Beddows, A. M. Jones, A. Calvo, C. Alves, and C. Pio (2013), An evaluation of some issues regarding the use of aethalometers to measure woodsmoke concentrations, *Atmos. Environ.*, *80*, 540–548, doi:10.1016/j.atmosenv.2013.08.026.

Haynes, W. M., and D. R. Lide (2011), *CRC Handbook of Chemistry and Physics: A Ready-Reference Book of Chemical and Physical Data*, CRC Press, Boca Raton, Fla.

Heintzenberg, J., and R. J. Charlson (1996), Design and applications of the integrating nephelometer: A review, *J. Atmos. Oceanic Technol.*, *13*(5), 987–1000, doi:10.1175/1520-0426(1996)013<0987:daaoti>2.0.co;2.

Herich, H., C. Hueglin, and B. Buchmann (2011), A 2.5 year's source apportionment study of black carbon from wood burning and fossil fuel combustion at urban and rural sites in Switzerland, *Atmos. Meas. Tech.*, *4*(7), 1409–1420, doi:10.5194/amt-4-1409-2011.

Jimenez, J., C. Cialborn, T. Larson, T. Gould, T. W. Kirchstetter, and L. Gundel (2007), Loading effect correction for real-time aethalometer measurements of fresh diesel soot, *J. Air Waste Manage.*, *57*(7), 868–873, doi:10.3155/1047-3289.57.7.868.

Kamboures, M. A., et al. (2013), Black carbon emissions in gasoline vehicle exhaust: A measurement and instrument comparison, *J. Air Waste Manage.*, *63*(8), 886–901, doi:10.1080/10962247.2013.787130.

Khan, B., M. D. Hays, C. Geron, and J. Jetter (2012), Differences in the OC/EC ratios that characterize ambient and source aerosols due to thermal-optical analysis, *Aerosol Sci. Technol.*, *46*(2), 127–137, doi:10.1080/02786826.2011.609194.

Lack, D. A., and C. D. Cappa (2010), Impact of brown and clear carbon on light absorption enhancement, single scatter albedo and absorption wavelength dependence of black carbon, *Atmos. Chem. Phys.*, *10*(9), 4207–4220, doi:10.5194/acp-10-4207-2010.

Lack, D. A., and J. M. Langridge (2013), On the attribution of black and brown carbon light absorption using the Angstrom exponent, *Atmos. Chem. Phys.*, *13*(20), 10,535–10,543, doi:10.5194/acp-13-10535-2013.

Lack, D. A., C. D. Cappa, E. S. Cross, P. Massoli, A. T. Ahern, P. Davidovits, and T. B. Onasch (2009), Absorption enhancement of coated absorbing aerosols: Validation of the photoacoustic technique for measuring the enhancement, *Aerosol Sci. Technol.*, *43*(10), 1006–1012, doi:10.1080/02786820903117932.

Lapuerta, M., R. Ballesteros, and F. J. Martos (2009), The effect of diesel engine conditions on the size and morphology of soot particles, *Int. J. Vehicle Des.*, *50*(1–4), 91–106.

Lewis, K., W. P. Arnott, H. Moosmuller, and C. E. Wold (2008), Strong spectral variation of biomass smoke light absorption and single scattering albedo observed with a novel dual-wavelength photoacoustic instrument, *J. Geophys. Res.*, *113*, D16203, doi:10.1029/2007JD009699.

Liu, Z. G., T. A. Swor, J. J. Schauer, J. A. Debilzen, and C. L. Severance (2008), A source dilution sampling system for characterization of engine emissions under transient or steady state operation, *Aerosol Sci. Technol.*, *42*(4), 270–280, doi:10.1080/02786820801992907.

Massabo, D., V. Bernardoni, M. C. Bove, A. Brunengo, E. Cuccia, A. Piazzalunga, P. Prati, G. Valli, and R. Vecchi (2013), A multiwavelength optical set-up for the characterization of carbonaceous particulate matter, *J. Aerosol Sci.*, *60*, 34–46, doi:10.1016/j.jaerosci.2013.02.006.

Park, S. S., A. D. A. Hansen, and S. Y. Cho (2010), Measurement of real time black carbon for investigating spot loading effects of aethalometer data, *Atmos. Environ.*, *44*(11), 1449–1455, doi:10.1016/j.atmosenv.2010.01.025.

Robinson, M. A., M. R. Olson, Z. G. Liu, and J. J. Schauer (2015), The effects of emission control strategies on light absorbing carbon emissions from a modern heavy duty diesel engine, *J. Air Waste Manage.*, *65*(6), 759–766, doi:10.1080/10962247.2015.1005850.

Robinson, M., G. Liu, M. Olson, and J. Schauer (2014), Comparison of measurement strategies for light absorbing aerosols from modern diesel engines, *SAE Int. J. Fuels Lubr.*, *7*(2), 543–550, doi:10.4271/2014-01-1570.

Russell, P. B., R. W. Bergstrom, Y. Shinozuka, A. D. Clarke, P. F. DeCarlo, J. L. Jimenez, J. M. Livingston, J. Redemann, O. Dubovik, and A. Strawa (2010), Absorption Angstrom exponent in AERONET and related data as an indicator of aerosol composition, *Atmos. Chem. Phys.*, *10*(3), 1155–1169, doi:10.5194/acp-10-1155-2010.

Sandradewi, J., A. S. H. Prevot, S. Szidat, N. Perron, M. R. Alfarra, V. A. Lanz, E. Weingartner, and U. Baltensperger (2008a), Using aerosol light absorption measurements for the quantitative determination of wood burning and traffic emission contributions to particulate matter, *Environ. Sci. Technol.*, *42*(9), 3316–3323, doi:10.1021/es702253m.

Sandradewi, J., A. S. H. Prevot, E. Weingartner, R. Schmidhauser, M. Gysel, and U. Baltensperger (2008b), A study of wood burning and traffic aerosols in an Alpine valley using a multiwavelength aethalometer, *Atmos. Environ.*, *42*(1), 101–112, doi:10.1016/j.atmosenv.2007.09.034.

Schauer, J. J., W. F. Rogge, L. M. Hildemann, M. A. Mazurek, G. R. Cass, and B. R. T. Simoneit (1996), Source apportionment of airborne particulate matter using organic compounds as tracers, *Atmos. Environ.*, *30*(22), 3837–3855, doi:10.1016/1352-2310(96)00085-4.

Schauer, J. J., et al. (2003), ACE-Asia intercomparison of a thermal-optical method for the determination of particle-phase organic and elemental carbon, *Environ. Sci. Technol.*, *37*(5), 993–1001, doi:10.1021/es020622f.

Schmid, O., P. Artaxo, W. P. Arnott, D. Chand, L. V. Gatti, G. P. Frank, A. Hoffer, M. Schnaiter, and M. O. Andreae (2006), Spectral light absorption by ambient aerosols influenced by biomass burning in the Amazon Basin. I: Comparison and field calibration of absorption measurement techniques, *Atmos. Chem. Phys.*, *6*, 3443–3462.

Schulz, M., et al. (2006), Radiative forcing by aerosols as derived from the AeroCom present-day and preindustrial simulations, *Atmos. Chem. Phys.*, *6*, 5225–5246.

Shen, G. F., Y. C. Chen, S. Y. Wei, X. F. Fu, Y. Zhu, and S. Tao (2013), Mass absorption efficiency of elemental carbon for source samples from residential biomass and coal combustions, *Atmos. Environ.*, *79*, 79–84, doi:10.1016/j.atmosenv.2013.05.082.

Singh, A., P. Rajput, D. Sharma, M. M. Sarin, and D. Singh (2014), Black carbon and elemental carbon from postharvest agricultural-waste burning emissions in the Indo-Gangetic Plain, *Adv. Meteorol.*, *10*, doi:10.1155/2014/179301.

Snyder, D. C., and J. J. Schauer (2007), An intercomparison of two black carbon aerosol instruments and a semi-continuous elemental carbon instrument in the urban environment, *Aerosol Sci. Technol.*, *41*(5), 463–474, doi:10.1080/02786820701222819.

Toon, O. B., J. B. Pollack, and B. N. Khare (1976), Optical constants of several atmospheric aerosol species: Ammonium sulfate, aluminum oxide, and sodium chloride, *J. Geophys. Res.*, *81*(33), 5733–5748, doi:10.1029/JC081i033p05733.

Utry, N., T. Ajtai, A. Filep, M. D. Pinter, A. Hoffer, Z. Bozoki, and G. Szabo (2013), Mass specific optical absorption coefficient of HULIS aerosol measured by a four-wavelength photoacoustic spectrometer at NIR VIS and UV wavelengths, *Atmos. Environ.*, *69*, 321–324, doi:10.1016/j.atmosenv.2013.01.003.

Virkkula, A., T. Makela, R. Hillamo, T. Yli-Tuomi, A. Hirsikko, K. Hameri, and I. K. Koponen (2007), A simple procedure for correcting loading effects of aethalometer data, *J. Air Waste Manage.*, *57*(10), 1214–1222, doi:10.3155/1047-3289.57.10.1214.

Wang, Q., R. J. Huang, J. Cao, Y. Han, G. Wang, G. Li, Y. Wang, W. Dai, R. Zhang, and Y. Zhou (2014), Mixing state of black carbon aerosol in a heavily polluted urban area of China: Implications for light absorption enhancement, *Aerosol Sci. Technol.*, *48*(7), 689–697, doi:10.1080/02786826.2014.917758.

Wang, Y., J. Y. Huang, T. J. Zananski, P. K. Hopke, and T. M. Holsen (2010), Impacts of the Canadian forest fires on atmospheric mercury and carbonaceous particles in northern New York, *Environ. Sci. Technol.*, *44*(22), 8435–8440, doi:10.1021/es1024806.

Wang, Y., P. K. Hopke, O. V. Rattigan, and Y. Zhu (2011), Characterization of ambient black carbon and wood burning particles in two urban areas, *J. Environ. Monit.*, *13*(7), 1919–1926, doi:10.1039/C1EM10117J.

Wang, Y., P. K. Hopke, O. V. Rattigan, D. C. Chalupa, and M. J. Utell (2012), Multiple-year black carbon measurements and source apportionment using Delta-C in Rochester, New York, *J. Air Waste Manage.*, *62*(8), 880–887, doi:10.1080/10962247.2012.671792.

Weingartner, E., H. Saathoff, M. Schnaiter, N. Streit, B. Bitnar, and U. Baltensperger (2003), Absorption of light by soot particles: Determination of the absorption coefficient by means of aethalometers, *J. Aerosol Sci.*, *34*(10), 1445–1463, doi:10.1016/s0021-8502(03)00359-8.

Yelverton, T. L. B., M. D. Hays, B. K. Gullett, and W. P. Linak (2014), Black carbon measurements of flame-generated soot as determined by optical, thermal-optical, direct absorption, and laser incandescence methods, *Environ. Eng. Sci.*, *31*(4), 209–215, doi:10.1089/ees.2014.0038.